Nuclear Engineering Design 62 (1980) 349–359

PRESSURE DROP AND VELOCITY DISTRIBUTION IN ROD BUNDLES WITH SPACER GRIDS

K. REHME
Kernforschungszentrum Karlsruhe, Institut für Neutronenphysik und Reaktortechnik, D-7500 Karlsruhe 1, Postfach 3640, Fed. Rep. Germany

G. TRIPPE
Kernforschungszentrum Karlsruhe, Institut für Reaktorbauelemente, D-7500 Karlsruhe 1, Postfach 3640, Fed. Rep. Germany

Received 11 July 1979

The paper contains experimental data and analysis of the pressure drop of turbulent flow through rod bundles. For laminar flow the dependence of the pressure drop on the pitch-to-diameter and wall-to-diameter ratios is discussed on the basis of theoretical analysis. In addition, correlations for the calculation of the pressure loss due to spacer grids are presented and compared with experimental data.

Detailed measurements of the velocity distribution in a full bundle of 19 rods are compared with predictions for fully developed turbulent flow. Moreover, detailed measurements of the velocity distributions upstream and downstream of spacer grids typical for LMFBRs are discussed together with the mass flow separation and redistribution between the subchannels. The mass flow distribution found experimentally is compared with the predictions by a subchannel code. The status of experimental knowledge is shown.

1. Introduction

Thermo- and fluid dynamic design calculations of LMFBR subassemblies are performed by subchannel analysis. The results computed by the subchannel codes (e.g. MISTRAL-II [1] and ARTIS [2]) essentially depend on the empirical input incorporated into the codes. The mass flow distribution between the different subchannels is affected by the pressure drop correlations and the turbulent mixing coefficients used in the codes. Moreover, the mass flow redistribution due to the different blockages of the subchannels by the spacer grids strongly depends on the assumptions for turbulent mixing and diversion cross flow. It is therefore most important to establish reliable empirical input for the codes which can only be achieved by experimental investigations. The aims of numerous experimental studies in the past were to obtain either empirical information as a direct input into the codes or detailed test data for comparison with computed results in order to adjust the codes against the measurements.

In the first part of this paper the pressure drop performance of rod bundles with longitudinal flow is discussed, based on both experimental studies and theoretical analysis for turbulent and laminar flow situations. In addition, correlations for the calculation of the important pressure losses of spacer grids are explained and compared with experimental results.

In the second part, the velocity and mass flow distribution in a rod bundle are discussed, for fully-developed turbulent flow and in the region affected by the partial blockage of the flow cross-section due to spacer grids. The status of different codes is shown by comparison with these experiment results. Further information is found by comparison with results of experimental investigations from the literature.

2. Pressure drop in rod bundles (K. Rehme)

2.1. Rod bundles without spacer grids

For the subchannel analysis the cross section of a rod bundle arranged in a hexagonal array is divided

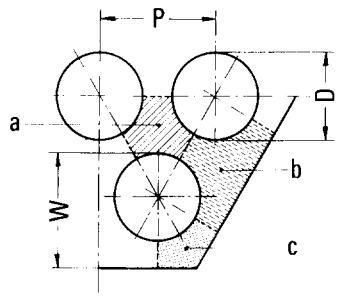

Fig. 1. Subchannels of rod bundles; (a) central, (b) wall, (c) corner.

into subchannels. Three different types of subchannels can be distinguished: central, wall and corner subchannel (fig. 1). The central and the corner subchannels are characterized by only one geometrical parameter: the pitch-to-diameter ratio P/D in case of the central subchannel and the wall-to-diameter ratio W/D for the corner subchannel. The wall subchannel, however, is characterized by two parameters: P/D and W/D. Flow in subchannels of rod bundles is one example where the equivalent diameter concept and the use of the friction factor correlations established for circular tubes can lead to unacceptable underpredictions or overpredictions of the friction factor. In this case it is not the error in the predicted overall pressure drop which is important, but the errors in the predicted mass-flow distributions between subchannels which can lead to erroneous predictions of the temperatures at the fuel pins.

2.1.1. Laminar flow

The pressure drop for fully developed laminar flow through straight ducts can be expressed by

$$\lambda \, \mathrm{Re} = K \,, \tag{1}$$

with the usual definitions of the friction factor

$$\lambda = \frac{\Delta p / \Delta L}{\frac{1}{2} \rho u^2 \, 1/d_\mathrm{h}} \tag{2}$$

and of the Reynolds number

$$\mathrm{Re} = \frac{\rho u d_\mathrm{h}}{\mu} \,. \tag{3}$$

The constant K in eq. (1) is a geometry parameter that

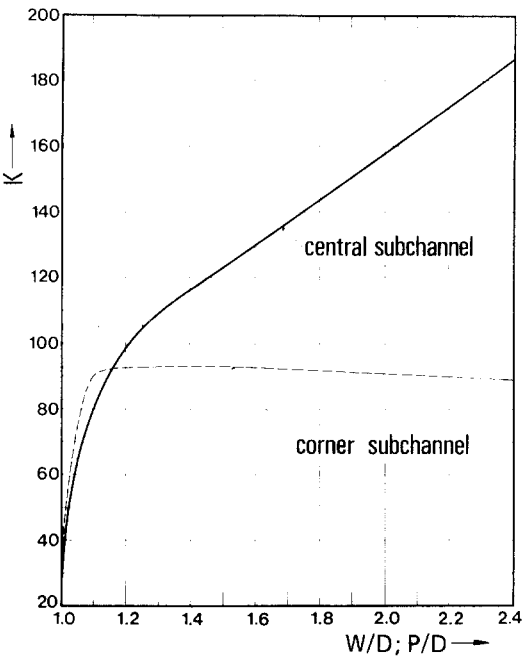

Fig. 2. Pressure drop in central and corner subchannels for laminar flow.

only depends on the configuration of the channel. K was calculated for subchannels of rod bundles over a wide range of P/D and W/D, respectively, [3], by solving the Poisson equation by the computer code DIXY [4].

Fig. 2 shows the results for central subchannels as a function of P/D and for corner subchannels as a function of W/D, respectively. The results for the central subchannels are in close agreement with the results of Sparrow and Loeffler [5]. The computed K-values for wall subchannels depending on P/D *and* W/D are plotted in fig. 3 as contours of constant K-values.

These values can be used as direct input into the codes for the different types of subchannels. However, it is also possible to calculate the K-values of rod bundles of any size. Under the conditions of (1) the same pressure drop in all subchannels, and (2) continuity, i.e. the total mass flow rate is equal to the sum of the individual mass flow rates, we get

$$\frac{1}{K_\mathrm{tot}} = \sum_i \frac{1}{K_i} \left(\frac{S_\mathrm{tot}}{S_i} \right)^2 \left(\frac{F_i}{F_\mathrm{tot}} \right)^3 \,, \tag{4}$$

where S is the wetted perimeter and F the flow cross-

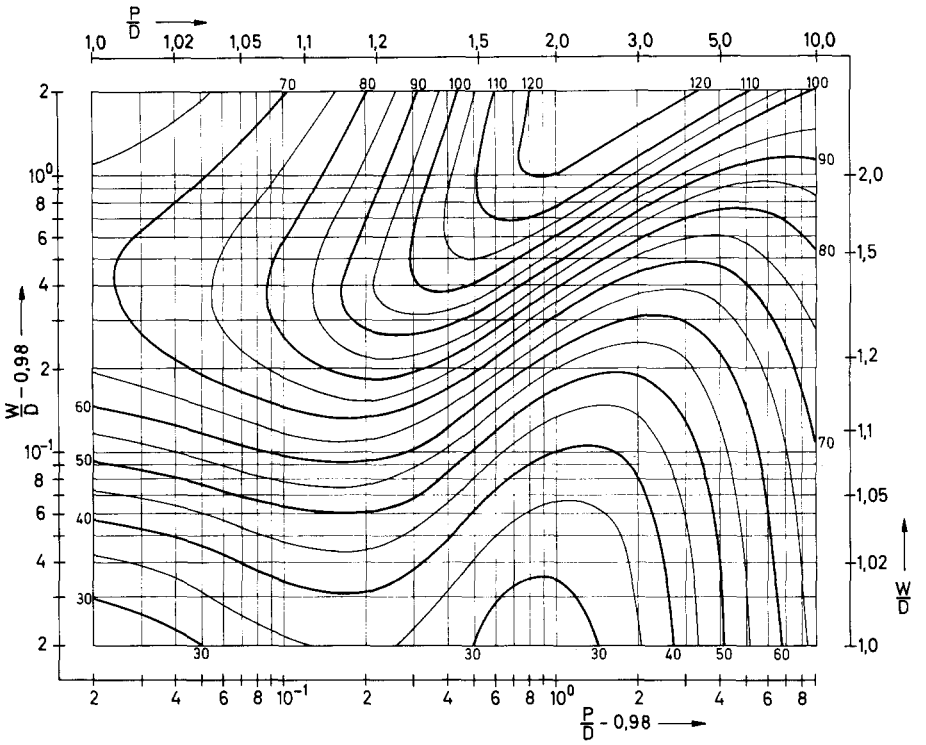

Fig. 3. Pressure drop in wall subchannels for laminar flow.

section, and the subscripts i are for the individual subchannels and 'tot' for the total rod bundle. A comparison between experimental K-values and those computed by eq. (4) shows a good agreement [3]. Moreover, a comparison between the K-values calculated by eq. (4) from the K-values of the individual subchannels with K-values computed for finite rod bundles of different sizes shows a maximum deviation of only 1.41% for a range of $1.105 \leqslant P/D \leqslant 2.06$ and $1.01 \leqslant W/D \leqslant 2.06$ [6].

2.1.2. Turbulent flow

In the case of turbulent flow, experimental information on friction factors of the subchannels of rod bundles and their dependence on P/D and W/D is very poor. The main reason for this lack of information is that experimental investigations are time-consuming, since both the wall shear stress distribution and the individual mass flow rate through the subchannel have to be measured. However, a method was developed to predict the friction factors for turbulent flow through non-circular channels on the basis of K-values for laminar flow [7]. Two empirical factors A and G^* can be determined from diagrams [7] and the friction factor for turbulent flow can be calculated from

$$\sqrt{\frac{8}{\lambda}} = A\,[2.5 \ln \mathrm{Re}\sqrt{\lambda/8} + 5.5] - G^* \,. \tag{5}$$

The factors A and G^* are only functions of K.

This method was shown to give satisfactory results of friction factors for different noncircular channels. A comparison between the few experimental friction factors and those predicted by eq. (5) is shown in table 1. All predicted friction factors are in very good agreement with the experimental ones based both on measurements of the pressure drop (Δp) and of the wall shear stress distribution (τ_w).

The friction factors of central subchannels and $P/D > 1.2$ can also be predicted with good approximation from the 'equivalent' annular zone solution [13]. The friction factor, λ, related to the friction factor of circular tubes, λ_t [14]:

$$\frac{1}{\sqrt{\lambda_t}} = 2.035 \log \overline{\mathrm{Re}}\sqrt{\lambda_t} - 0.989 \tag{6}$$

Table 1
Comparison between predicted and experimental friction factors of subchannels of rod bundles; test fluid = air

Type of subchannel	P/D	W/D	K	A	G *	Re × 10^{-5}	λ_E/λ_C Δp	λ_E/λ_C τ_W	Ref.
Central	1.217	–	102.7	1.0	6.160	1.5–3.7	1.010 [a]		[8]
Wall	1.071	1.072	58.3	1.02	5.64	0.873	1.014	1.020	[9]
Wall	1.148	1.148	79.4	1.0	5.883	1.23	0.988	0.990	[10]
Wall	1.402	1.401	103.5	1.0	6.165	1.94	0.987	1.001	[11]
Corner	–	1.072	64	1.0	5.699	0.597	–	1.013	[12]

[a] Based on Δp, τ_W and hot wire measurements and averaged over the Reynolds number range tested.

can be expressed as [13]

$$\frac{\lambda}{\lambda_t} = 1.045 + 0.071(P/D - 1)$$

$$\text{for } \overline{Re} = 10^4 \ , \tag{7}$$

$$\frac{\lambda}{\lambda_t} = 1.036 + 0.054(P/D - 1)$$

$$\text{for } \overline{Re} = 10^5 \ . \tag{8}$$

2.2. Pressure drop of spacer grids

The pressure drop at the spacer grids of a LMFBR fuel subassembly is of the same order of magnitude as the pressure drop due to friction at the walls of the fuel elements and the wrapper tube. The pressure drop of spacer grids, of course, depends on the design of the spacer grid under consideration. However, experiments on the pressure drop of spacer grids of very different designs showed that the partial blockage of the flow cross section is the main parameter which affects the pressure drop [15,16,17]. The drag coefficient ζ of a spacer grid

$$\Delta p_g = \zeta \frac{\rho}{2} u^2 \tag{9}$$

can be modified by relating the drag coefficient to the relative blockage of the flow cross section ϵ

$$\epsilon = F_B/F \tag{10}$$

to

$$\zeta = C_v \cdot \epsilon^2 \ . \tag{11}$$

The relative blockage is defined as the cross-section blocked in the axial direction divided by the undisturbed flow cross-section. The experimental results indicated that the modified drag coefficient C_v can be expressed as [16]

$$C_v = 6 \div 7 \ , \text{ for } Re > 5 \times 10^4$$

and short spacer grids with leading edges well rounded and a range of blockage ratios of $0.2 \leqslant \epsilon \leqslant 0.45$. Thus, for design calculations the pressure drop of spacer grids may be calculated by eq. (11) and (12) with good approximation.

However, besides the blockage ratio, the length of the spacer grid, and more importantly the leading edge of the spacer grid, also influence the drag coefficient. This was shown in a recent experiment on the pressure drop of spacer grids in a bundle of 12 rods [18]. Fig. 4 shows some of the results of this investigation.

To influence the drag coefficient of the original grid design (SI) the leading edge was chamfered. Because of the burr caused by the working process this

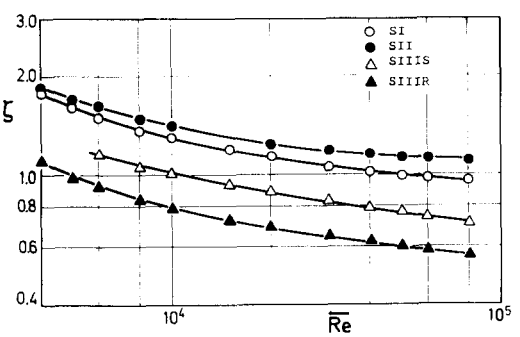

Fig. 4. Drag coefficients of spacer grids versus the Reynolds number.

resulted in an increase in the drag coefficient (SII). As a consequence, the blockage of the flow cross-section by the grid of $\epsilon = 0.348$ (SI and SII) was reduced to $\epsilon = 0.28$ (SIII). Despite a sharp leading edge, the drag coefficient was reduced considerably (SIIIS) due to the reduced blockage. Rounding of the leading edge (SIIIR) greatly reduced the drag coefficient even further.

2.3. Conclusions

Pressure drop correlation for fully developed flow is established for both turbulent and laminar flow through rod bundles with an accuracy sufficient for design purposes. It is recommended to use the correlations based on eq. (5) for the prediction of the pressure drop in subchannels of rod bundles for turbulent flow. There is only poor information on the pressure drop in the transition between laminar and turbulent flow and for developing flows.

The pressure loss due to the spacer grids can be computed using eq. (11) as an approximation, Spacer grids can be very different in design, therefore experimental investigation is necessary to find the accurate pressure loss of a spacer grid.

3. Velocity and mass flow distribution in rod bundles with and without spacer grids (G. Trippe)

3.1. Experimental and theoretical investigations

To support the methods used to calculate the local velocity fields as well as the global mass flow distributions in multirod bundles, experiments were performed in a bundle of 19 hexagonally arranged rods ($P/D = 1.30$; $W/D = 1.17$). The main data of this test section are listed in table 2.

Local velocity fields were measured by means of Pitot tubes in a turbulent water flow ($15\,000 \leqslant \mathrm{Re} \leqslant 90\,000$) for complete bundle cross sections. From these time-averaged axial velocity fields the mean velocities and the mass flow rates of the characteristic subchannels of the 19-rod-bundle (corner, wall, central subchannels) were evaluated. The experiments were carried out in bundles with and without grid-type spacers.

The results were compared both with other experimental investigations of different geometries known from the literature and with calculated values of theoretical investigations with available codes.

Table 2
Main data of the bundle test section; test fluid = water

Number of rods	19
Rod arrangement	Hexagonal
Rod diameter (mm)	$D = 25{,}0$
Characteristic ratios	$P/D = 1{,}30$
	$W/D = 1{,}17$
Hydraulic diameters (mm)	
Central subchannel	$d_h = 21{,}9$
Wall subchannel	$d_h = 16{,}8$
Corner subchannel	$d_h = 8{,}5$
Bundle (averaged)	$D_h = 18{,}42$
Fluid employed	water

In the following the main results from earlier detailed studies [19,20] are summarized. Portions were presented in earlier publications [21,22,23].

3.2. Fully developed turbulent flow in rod bundles

The undisturbed, fully-developed flow distribution has to be determined as the reference condition for the more complicated three-dimensional flows in realistic reactor bundles. For the experimental investigations, a test section was chosen with subchannels of rather different hydraulic diameters (table 2), to obtain mass flow rates in the subchannels which differ greatly. In fig. 5, the experimental results for $\overline{\mathrm{Re}} = 60\,000$ are plotted as a field of normalized isotaches u/U for a 30° section of the 19-rod bundle. In addition computed results are shown calculated by means of the VELASCO code [24] and the VITESSE code [25]. The comparison shows quite good agreement, generally. The maximum deviation of local velocities is 3% (fig. 5), of mean subchannel velocities even 1%, which is shown in table 3. However, recalculations by means of the subchannel code ARTIS [2] were less satisfactory, the deviations amounting to 5% (table 3).

With the first calibration test for codes within a complete, realistic bundle cross-section it was possible to prove that these two local codes are able to calculate the undisturbed and fully developed flow distribution for fuel elements with similar geometrical conditions as used in the experiments. However, further

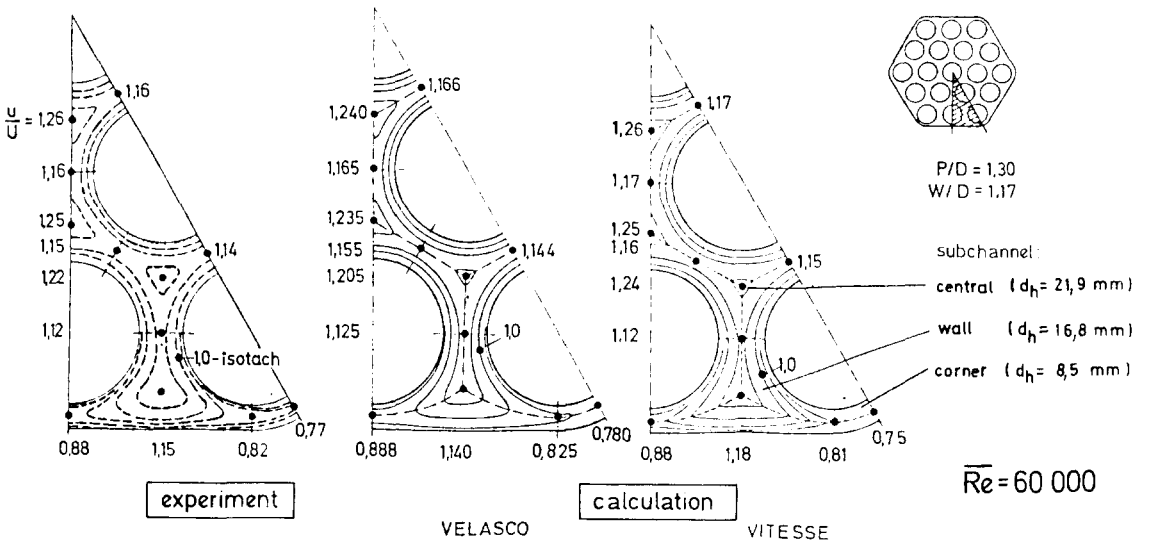

Fig. 5. Fully developed velocity distribution in a 19-rod bundle ($\overline{Re}$ = 60 000, P/D = 1,30, W/D = 1,17); comparison between experiment and calculations.

investigations show that the agreement is less satisfactory, both with decreasing Reynolds numbers and for rod bundles with very small pitch-to-diameter ratio ($P/D \leqslant 1.10$) [19,20].

The local velocity distribution normal to the pin wall in bare rod bundles is in agreement with the law of the wall known from investigations in circular tubes [26]. In azimuthal direction, however, the velocity variation depends on the geometry of the subchannel and the Reynolds number. For these conditions new empirical relations have been found [19,20]. As example, fig. 6 shows the azimuthal velocity variation

Table 3
Comparison between experimental and computed mean subchannel velocities in the 19-rod bundle for fully developed flow at $\overline{Re}$ = 60 000

		Experiment	VELASCO	VITESSE	ARTIS
	(subchannel)				
$\bar{u}_1/U$	(corner)	0.67	0.682	0.662	0.670
$\bar{u}_2/U$	(wall)	0.94	0.940	0.945	0.895
$\bar{u}_3/U$	(first central)	1.06	1.053	1.055	1.085
$\bar{u}_{(4+5)}/U$	(inner central)	1.07	1.075	1.074	1.108

Deviations from experiment	$\% \cdot U$		
Corner channel (No. 1)	+1	−1	0
Wall channel (No. 2)	0	0	−5
First central channel (No. 3)	0	0	+3
Inner central channel (No. 4 + 5)	0	0	+3

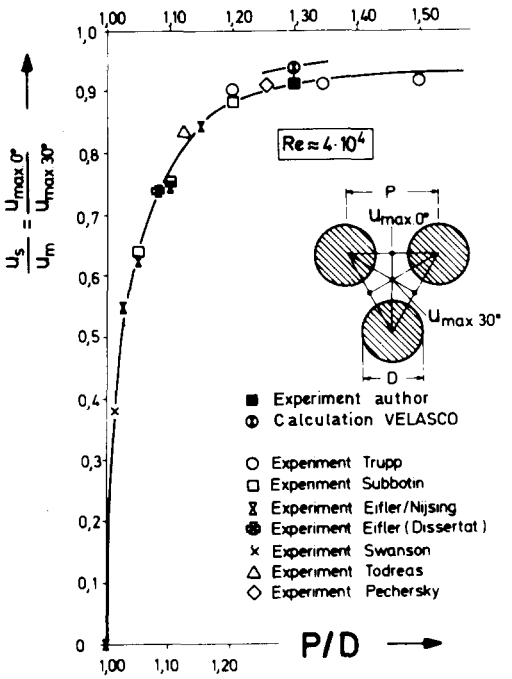

Fig. 6. Azimuthal velocity variation in rod bundle subchannels versus the pitch-to-diameter ratio (Re ≈ 40 000).

of a central subchannel characterized by the velocity ratio u_s/u_m, as a function of the P/D-ratio of the bundle. All available experimental data from the literature were used to derive this functional dependence [27–33], including water and air [31].

Results computed by VELASCO and VITESSE deviate from the empirical relations $u_s/u_m = f(P/D)$ and $u_s/u_m = f(\mathrm{Re})$ [19,20]. Therefore the codes should be improved.

A correlation for the mass flow distribution in rod bundles presented in [31] has been improved based on these new and more precise results [19,20].

3.3. Spacer grid influences on flow in rod bundles

Spacer grids not only disturb the local velocity fields but also affect the mass flow distribution in a rod bundle if the subchannels are different blocked. In reactor core design the coolant mass flow in a bundle should be directed from the normally over-cooled side zone to the under-cooled central zone. A quantitative correlation between spacer geometry, i.e., blocked area in the side zone, and mass flow separation and its redistribution was found to be a main problem in thermohydraulic bundle design. The complete three-dimensional flow distribution in the 19 rod bundle with spacer grids was therefore investigated.

A complete set of local axial velocity fields was obtained from detailed measurements in the bundle cross section upstream and downstream from spacer grids for LMFBRs. From these results the cross flows could be determined.

3.3.1. Local velocity distributions in gridded rod bundles

To demonstrate the influence of the spacer grid on the local axial velocity distributions a set of velocity profiles at different axial distances between the measuring plane and the spacer grid (L/D_h) was measured. The results are plotted in fig. 7 as measured velocity relations $(u/U)^2$ across the symmetry line M of a wall and a central subchannel. The axial lengths behind the spacer grid was investigated from $L/D_h = 0.06$ to $L/D_h = 50$.

As can be seen, for the region $0.06 \lesssim L/D_h \lesssim 10$, the profiles reveal individual disturbances (wakes) in

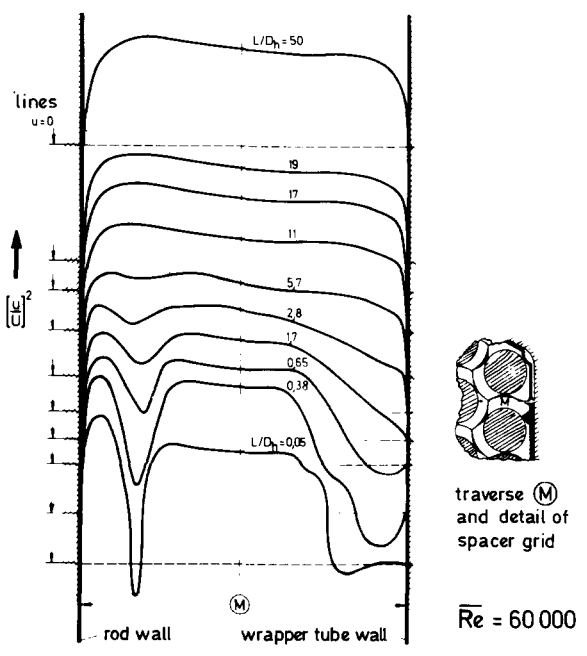

Fig. 7. Measurements of axially developing velocity profiles downstream of the spacer grid ($\overline{\mathrm{Re}}$ = 60 000).

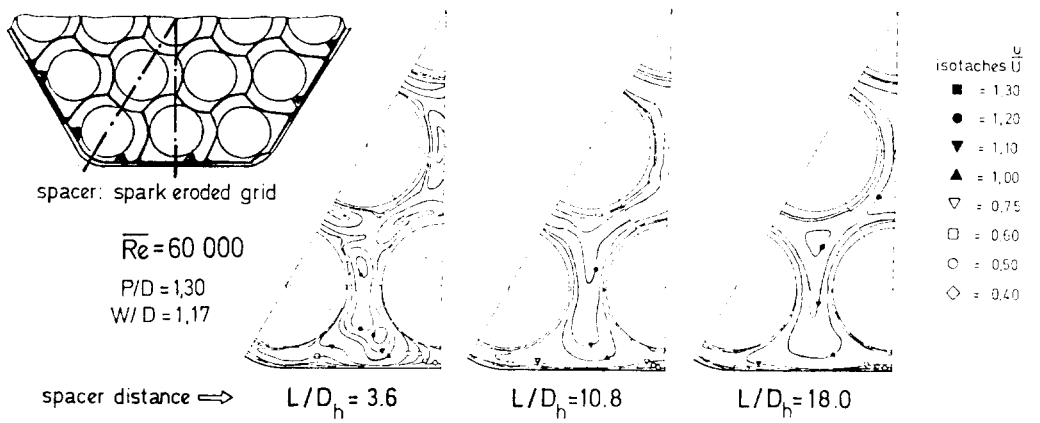

Fig. 8. Axially developing velocity fields in a 19-rod bundle downstream of the spacer grid ($\overline{Re}$ = 60 000).

the velocity distributions just behind the spacer structure. These wake zones disappear gradually with increasing L/D_h and the velocity profile is approximately redistributed at $L/D_h \approx 10$. To arrive at a nearly fully developed velocity profile needs an additional axial length of $L/D_h \approx 40$.

More information is obtained from detailed velocity field measurements in the complete bundle cross section at different distances from the spacer grid. Some of those measured results are plotted in fig. 8 as normalized isotaches u/U for a 30° sector of the bundle. The following can be seen:

(a) For L/D_h = 3.6 a deformed structure of the velocity distribution was registered due to the spacer geometry. Knowing this geometry, the trends of the individual isotaches can be explained.

(b) This very irregular velocity structure is gradually smoothed out with increasing L/D_h, as can be seen from the respective plots for L/D_h = 10.8 and for L/D_h = 18.

(c) At L/D_h = 18 a fairly uniform structure of the isotaches was measured. At this axial length the individual subchannel flow seems to be established, but a flow redistribution across the whole bundle still exists.

(d) The differences between the isotach fields at L/D_h = 18 and the undisturbed case (fig. 5) mainly exist in the enlargement of the isotachs in the wall and corner channels and their reduction in the central channels with increasing L/D_h.

In [19], additional and more detailed local velocity fields are presented. By intercomparing these fields it is possible to determine the local effects of the flow redistribution. Some characteristics have been evaluated.

The influence of the Reynolds number on the local velocity distribution was investigated as well. For this reason, experiments were carried out at $\overline{Re}$ = 30 000 and $\overline{Re}$ = 60 000. A typical result is shown in fig. 9, which compares normalized velocity profiles across the symmetry line M of the interconnected wall and central subchannels. Only the maximum velocity increases by 2% with decreasing Reynolds number. This is due to the known Re number effect on the local velocity distribution within subchannels. It can be concluded that the Re number is of minor influ-

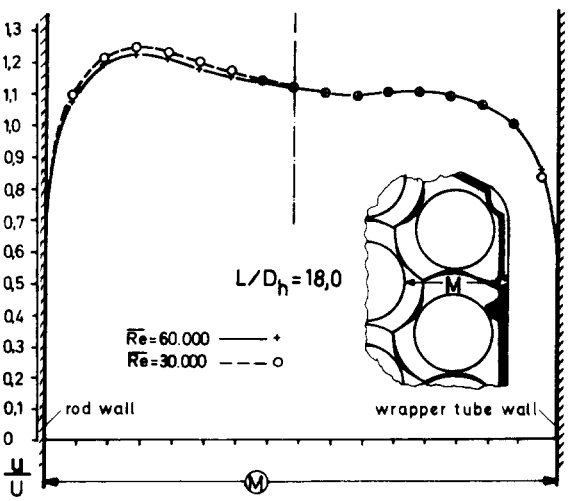

Fig. 9. Influence of Re number on flow distribution in gridded rod bundles.

ence on the flow distribution in gridded rod bundles within the investigated Reynolds number region. Intercomparisons of mass flow distributions show the same result [19].

3.3.2. Mass flow distributions in gridded rod bundles

As seen from fig. 8, by intercomparing the isotache fields, coolant mass flow is displaced from the side channels due to the higher blockage in the side subchannels. This displaced mass redistributes downward the spacer. To obtain quantitative data the mass flows in the individual subchannels were evaluated by integration of the local velocity fields measured at different axial position L/D_h.

The displacement and redistribution of mass flows in the subchannels 1*, 2*, 3*, 4 and 5 is shown in fig. 10, where the mass flow rates are plotted versus the nondimensional axial length upstream and downstream of the spacer grid. As shown in [19], mass flows in subchannels 1 and 2 differ slightly from those in 1* and 2* due to the nonsymmetrical geometry of this spacer type in the side channels (fig. 8).

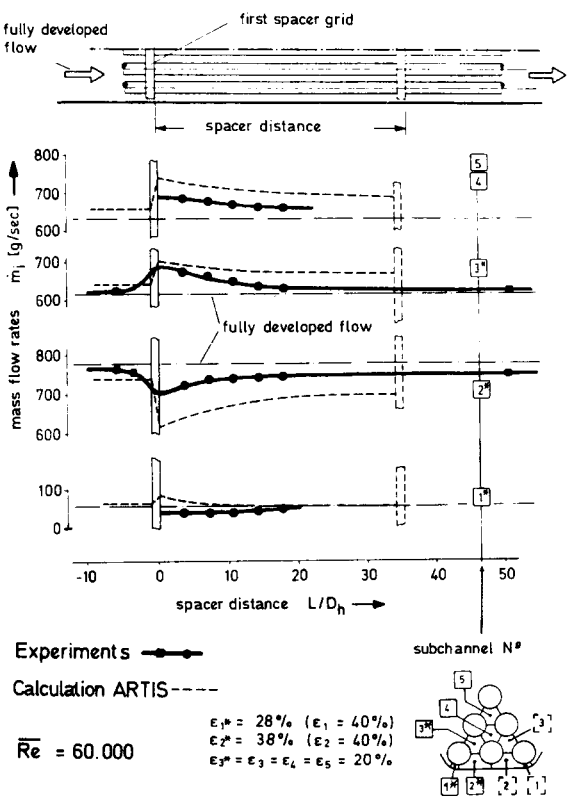

Fig. 10. Mass flow distribution in a 19-rod bundle with spacer grid ($\overline{Re}$ = 60 000); comparison between experiment and calculation.

The different blockages in the subchannels give rise to a remarkable change in the mass flow rates of the subchannels. The separation and the redistribution caused by the spacer from the higher blocked side subchannels (39%) into the less blocked central channels (20%) can be clearly recognized. The change in mass flow directly at the spacer is 14% of the overall mass flow in the side zone, which gives the height for the crossflow into the central zone.

About 10 D_h downstream this change has decreased to half its maximum value. Further redistribution is a very slow process; 50 D_h downstream only about 70% of the initial displaced mass has been redistributed. Under LMFBR conditions with a distance between the spacers of about 35 D_h this means that a preceeding spacer grid acts upon the following one. The upstream effect of the spacer grid reaches about 5 D_h which can also be seen from fig. 10. Thus, this spacer type alters the mean mass flow in the side zone by 6% within the axial mean of the first spacer distance.

In addition to the experimentally determined mass flow curves, the corresponding curves calculated by the subchannel code ARTIS have been plotted as dashed lines. It appears that for qualitatively similar curves, quantitative differences occur mostly in the wall channel and the central channels 3*, 4 and 5. For the corner subchannel there is qualitative error because the upstream effect of the spacer grid is neglected. Due to the lower or higher mass flow rates in the undisturbed state upstream of the spacer (see table 3) and the higher change of mass flow at the spacer itself, mean flow rates of less than about 15% for subchannel 2* and flow rates higher than about 10% for subchannels 3*, 4 and 5 with respect to the experiments are obtained as values averaged over the axial spacer distance (35 D_h). The deviation in crossflow from the side to the central zone amounts to a factor 2 for this spacer type.

First improvements of ARTIS [22] are not satisfactory. More general corrections and new models have to be introduced in this 3-dimensional code.

Summarizing, it can be stated that the global calculation using the ARTIS-code yields qualitatively

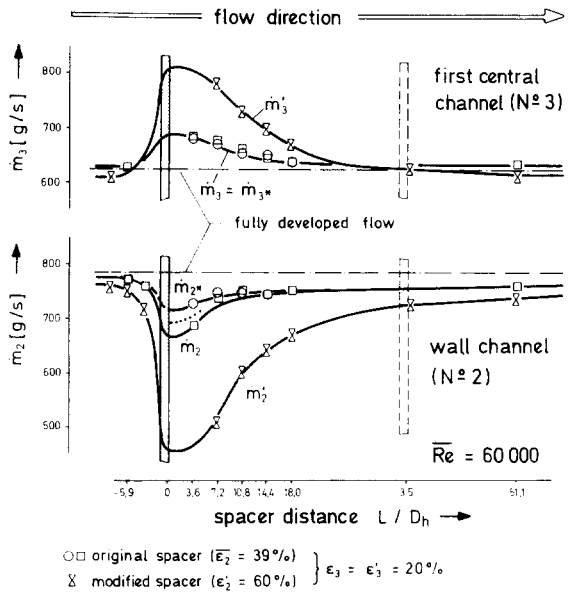

Fig. 11. Mass flow distribution with varying spacer grid blockages in the side zone of a 19-rod bundle ($\overline{Re}$ = 60 000).

similar mass redistributions as these experiments, but clear quantitative deviations in bundles with spacer grids. Therefore this and similar computer codes should be fitted now with priority, since the velocity distribution exerts a significant influence on the temperature distribution within bundles.

To develop a correlation between the mass flow separation and the spacer grid geometry further experimental investigations were performed. As one result it was found that the height of the spacer grid is of minor influence on the mass flow separation [19]. However, the magnitude of the blocked area in the side zone is of remarkable influence. That is shown in fig. 11 as an example. The corresponding mass flow curves are plotted for a spacer with a higher blockage in the side zone (60% instead of 39%), both for the wall and the adjacent central subchannel. In this case the mass flow separation is three times that of the original spacer. More details of these investigations can be found in [19].

These results constitute important findings with respect to the most suitable design of spacers. A correlation is presented in [19] between the maximum cross flow from the side into the central zone and the blockage due to the spacer in the range of 20% to 100%. A corresponding correlation is given for the mean mass flow reduction in the side zone within the axial mean of the first spacer distance. Experiments with a second spacer installed 35 D_h downstream of a first one showed that the same flow separation occurs at the second spacer [19]. Further experimental investigations are necessary to evaluate quantitative correlations describing the flow distributions for series of alternating spacers installed in a bundle geometry.

3.4. Conclusions

As results of these studies [19,20] the following statements can be made:

(a) the mass flow and velocity distributions in rod bundles with fully developed turbulent flow are well known; empirical correlations for local velocity and mass flow distribution are now available;

(b) three-dimensional flows in bundles with actual spacer grids could be well detected by complete sets of experimental data; the main effects are now understood;

(c) for coolant flow separation and redistribution between side and central zones of a bundle with P/D = 1.30, quantitative correlations are available now for the spacer design used in these experiment;

(d) testing of calculation methods showed that the local codes VELASCO and VITESSE can predict the two-dimensional, fully developed flow in bare rod bundles quite well for $P/D \geq 1.1$ and $\overline{Re} > 5 \times 10^4$; three-dimensional SUBCHANNEL codes have to be verified now by comparison with the experimental results.

Problems still open are:

(1) correction factors for bundles with $P/D < 1.2$ and for distorted bundle geometries (non-nominal);

(2) bundle entrance effects;

(3) reproducing of mass flow separation with series of alternating spacer grids;

(4) calibration of codes, especially the three-dimensional codes.

To solve these problems corresponding experimental investigations are in preparation at KfK.

Nomenclature

A	geometry parameter: turbulent flow
C_v	modified drag coefficient

D	diameter of the rod(m)
D_h	hydraulic diameter, bundle average (m)
F	flow cross-section (m^2)
G^*	geometry parameter: turbulent flow
K	geometry parameter: laminar flow
L	distance from downstream end of the spacer grid (m)
ΔL	length (m)
$\dot{m}$	mass flow rate ($kg\ s^{-1}$)
P	pitch of the rods (mm)
Δp	pressure loss (Nm^{-2})
$\overline{Re}$	Reynolds number, bundle average
Re	Reynolds number
S	wetted perimeter (m)
U	mean velocity in a bundle (ms^{-1})
$\overline{u}$	mean velocity in a subchannel (ms^{-1})
W	distance from the wrapper tube (m) (fig. 1)
ζ	drag coefficient
ϵ	blockage ratio
λ	friction factor
μ	viscosity ($kg\ m^{-1}s^{-1}$)
ρ	density ($kg\ m^{-3}$)

Subscripts

C	calculated
E	experimental
g	spacer
i	individual subchannel
m	maximum
s	gap maximum
t	tube
tot	total

References

[1] W. Baumann, Report KfK 1605 (1972) (in German).
[2] G. Straub, Calculation of temperature and velocity fields for parallel flow through sodium-cooled fast reactor fuel elements, Dissertation TU Stuttgart, 1976 (in German)
[3] K. Rehme, Chem. Ing. Techn. 43 (1971) 962–966 (in German).
[4] W. Höbel, DIXY, Proc. GAMM-Workshop on Fast Solution Methods for the Discretized Poisson Equation, Karlsruhe, March 3–4, 1977 (Advance Publishers, London, 1978) pp. 199–216.
[5] E.M. Sparrow and A.L. Loeffler, AIChE J. 5 (1959) 325–330.
[6] R. Ullrich, Report TUBIK 36 (1974) (in German).
[7] K. Rehme, Internat. J. Heat Mass Transfer 16 (1973) 933–950.
[8] B. Kjellström, Report AE-487, Studsvik (1974).
[9] K. Rehme, Nucl. Engrg. Des. 45 (1978) 311–323.
[10] K. Rehme, Report KfK-2617 (1978) (in German).
[11] K. Rehme, Report KfK-2637 (1978) (in German).
[12] K. Rehme, Report KfK-2512 (1977) (in German).
[13] K. Rehme, Internat. J. Heat Mass Transfer 15 (1972) 2499–2517.
[14] K. Maubach, Chem. Ing. Techn. 42 (1970) 995–1004 (in German).
[15] K. Rehme, ATKE 15 (1970) 127–130 (in German).
[16] K. Rehme, Nucl. Technol. 17 (1973) 15–23.
[17] K. Rehme, Nucl. Technol. 33 (1977) 314–317.
[18] K. Rehme, Report KfK 2697 (1978).
[19] G. Trippe, Experimentelle Untersuchungen turbulenter Strömungen in axial durchströmten Stabbündeln ohne und mit gitterförmigen Abstandshaltern; Report 2834 KfK und Dissertation Universität Karlsruhe, 1979, to appear.
[20] G. Trippe et al., Gesetzmässigkeiten der voll eingelaufenen, turbulenten Strömung in Stabbündeln und Bewertung verschiedener Auslegungsrechenprogramme.
[21] R. Möller, D. Weinberg, G. Trippe and H. Tschöke: IAEA-SM-225/34 (1978) 673–692.
[22] G. Trippe and D. Weinberg, experimental and theoretical investigations of turbulent velocity distribution in rod bundles with and without grid-type spacers, NATO-Advanced Study Institute on Turbulent Forced Convection in Channels and Rod Bundles, Istanbul, Turkey, 1978.
[23] G. Trippe et al., Fluiddynamische Untersuchungen an Bündelgeometrien; Untersuchungen der dreidimensionalen Geschwindigkeitsverteilung in H_2O-Strömung, Quarterly KfK-PSB (1978).
[24] W. Eifler and R. Nijsing, Report EUR-4950e (1973).
[25] W. Slagter, H.A. Roodbergen and N.H. Decker, Prediction of fully-developed turbulent flow in non-circular channels by the finite element method, NATO Advanced Study Institute, Istanbul, Turkey (1978).
[26] J. Nikuradse, VDI-Forschungsheft Nr. 356 (1932).
[27] A.C. Trupp and R.S. Azdad, Nucl. Engrg. Des. 32 (1975) 47–84.
[28] V.I. Subbotin, P.A. Ushakov, Yu. D. Levchenko and A.M. Alexandrov, Report AEC-tr-7189 (1971).
[29] W. Eifler and R. Nijsing, Report EUR-2193e (1965).
[30] W. Eifler, Über die turbulente Geschwindigkeitsverteilung und Wandreibung in Strömungskanälen verschiedener Querschnitte, Dissertation TH Darmstadt, 1968.
[31] L.D. Palmer and L.L. Swanson, GAMD-1335 (1960).
[32] P. Carajilescov and N.E. Todreas, Trans. ASME (May 1976) 262–268.
[33] M.J. Pechersky, R.M. Roidt, B.J. Vegter and R.A. Markley, Report WARD-OX-3045-6 (1974).